ADVANCED FUNCTIONAL MATERIALS
www.afm-journal.de

Design Rule Hidden from The Eye in S/N-Bridged Ancillary Ligands for Copper(I) Complexes Applied to Light-Emitting Electrochemical Cells

Ginevra Giobbio, Luca M. Cavinato, Elisa Fresta, Anaïs Montrieul, Gilbert Umuhire Mahoro, Jean-François Lohier, Jean-Luc Renaud, Mathieu Linares, Sylvain Gaillard, and Rubén D. Costa**

Enhancing low-energy emitting Cu(I)-ionic transition metal complexes (iTMCs) light-emitting electrochemical cells (LECs) is of utmost importance towards Cu(I)-iTMC-based white-emitting LECs. Here, the ancillary ligand design includes (i) extension of π-systems and (ii) insertion of S-bridge between heteroaromatics rings. This led to two novel heteroleptic Cu(I)-iTMCs: 2-(pyridin-2-yl-l2-azanyl)quinoline (CuN2) and 2-(naphthalen-2-ylthio)-quinoline (CuS2) as N^N and bis[(2-diphenylphosphino)phenyl] ether as P^P,-exhibiting improved photoluminescence quantum yields (ϕ) and thermally activated delayed fluorescence processes compared to their reference Cu(I)-iTMCs: di(pyridin-2-yl)-l2-azane (CuN1) and di(pyridin-2-yl)sulfane (CuS1). Despite CuS2 stands out with the highest ϕ (38% vs 17 / 14 / 1% for CuN1 / CuN2 / CuS1), only CuN2-LECs show the expected enhanced performance (0.35 cd A^{-1} at luminance of 117 cd m^{-2}) compared to CuN1-LECs (0.02 cd A^{-1} at6 cd m^{-2}), while CuS2-LECs feature low performances (0.04 cd A^{-1} at 10 cd m^{-2}). This suggests that conventional chemical design rules are not effective towards enhancing device performance. Herein, nonconventional multivariate statistical analysis and electrochemical impedance spectroscopy studies allow to rationalize the mismatch between chemical design and device performance bringing to light a hidden design rule: polarizability of the ancillary ligand is key for an efficient Cu(I)-iTMC-LECs. All-in-all, this study provides fresh insights for the design of Cu-iTMCs fueling research on sustainable ion-based lighting sources.

1. Introduction

Among the thin-film lighting technologies arisen in the past decades, light-emitting electrochemical cells (LECs) stand out by the simplest device architecture (single-layered vs multilayered devices) and the easiest device fabrication (solvent-based deposition techniques under ambient conditions), making them cheap and attractive for large-scale preparation in moderate performing lighting applications.[1] These assets are attributed to the presence of mobile ions in the active layer, leading to (i) an efficient ion-assisted charge injection upon biasing by forming electric double layers (EDLs) at the electrode interfaces, (ii) a controlled growth of the p-/n-doped fronts, and (iii) an electron–hole recombination limited at the intrinsic neutral zone (*i*) of a dynamically formed p–*i*–n junction.[2–5] These processes have shown a great tolerance in terms of device 3D-shapes and architectures as well as device fabrication techniques.[6]

As prior-art, the best performing LECs have been reached with expensive and high supply-risk emitters, such asIr(III)-based ionic transition metal complexes or

G. Giobbio, L. M. Cavinato, E. Fresta, R. D. Costa
Technical University of Munich, Campus Straubing for Biotechnology and Sustainability
Chair of Biogenic Functional Materials
Schulgasse 22, 94315 Straubing, Germany
E-mail: ruben.costa@tum.de

The ORCID identification number(s) for the author(s) of this article can be found under https://doi.org/10.1002/adfm.202304668

DOI: 10.1002/adfm.202304668

G. Giobbio, A. Montrieul, G. Umuhire Mahoro, J.-F. Lohier, J.-L. Renaud, S. Gaillard
Normandie University
ENSICAEN
UNICAEN
CNRS
LCMT
14000 Caen, France
E-mail: sylvain.gaillard@ensicaen.fr

E. Fresta
Institute for Physical Chemistry
INF 253
Universität Heidelberg
69120 Heidelberg, Germany

Ir(III)-iTMCs.[7,8] As an alternative, the well-known Cu(I)-iTMCs have been catching more and more attention as low-cost, low-toxic, abundant, and sustainable emitters covering the whole visible spectrum.[9,10] Moreover, most of them have exhibited a thermally activated delayed fluorescence (TADF) emission mechanism that consists in harvesting both singlet and triplet excitons, allowing to reach device efficiencies up to 100%.[11–15] In the last decade, research has been focused on heteroleptic Cu(I)-iTMCs combining (i) sterically hindered P^P ligands, such as bis[(2-diphenylphosphino)phenyl] ether (DPEPhos) or 4,5-bis(diphenylphosphino)−9,9-dimethylxanthene (XanthPhos), and (ii) N^N bidentate ligands, such as bipyridine and dipyridylamine families.[6,9,16–20] While the bulkiness of the P^P prevents the flattening distortion at the excited state,[18,21] the N^N ligand rules the fine-tuning of photophysical properties, such as emission wavelength and photoluminescence quantum yields (ϕ), among others.[9,16,17] Though most of the reported examples have led to green- and yellow-emitting LECs,[22–26] there are a handful of ligand designs for blue-[27] and red-[21] emitting LECs featuring performances as high as 3.6 cd A^{-1} at luminance of 180 cd m^{-2} and 0.19 lm W^{-1} at irradiance of 130 μW cm^{-2}, respectively. This has recently allowed us to fabricate the first fully Cu(I)-iTMC-based white-emitting LECs with encouraging performances (0.6 cd A^{-1} at luminance of 30 cd m^{-2}) that are still limited by poorly emissive low energy-emitting complexes.[28]

In this context, we decided to explore the design of low-energy emitting complexes based on heteroleptic Cu(I)-iTMCs with archetypal DPEPhos as P^P and new N- or S-bridged N^N ligands following well-known chemical designs: (i) asymmetric extension of the π-conjugation[10,29] and (ii) introduction of S-bridge between the heteroaromatic rings.[9,10] This allowed us to fairly study the new complexes with the ligands 2-(pyridin-2-yl-l2-azanyl)quinoline (**CuN2**) and 2-(naphthalen-2-ylthio)quinoline (**CuS2**) in comparison with the known symmetric counterparts (i.e., di(pyridin-2-yl)-l2-azane (**CuN1**) and di(pyridin-2-yl)sulfane (**CuS1**); **Figure 1**). As expected, standard X-ray analysis, steady-state and temperature-dependent time-resolved emission spectroscopy, electrochemical assays, and density functional theory and their time-dependent (DFT and TD-DFT) computational studies confirmed that both approaches are effective with respect to red-shifting the emission wavelength maxima, keeping a TADF emission mechanism with enhanced radiative rate constant. Thus, LECs based on the asymmetric complexes should outperform those with symmetric complexes, while the best devices should be achieved with **CuS2** that features, for example, the highest ϕ value in the series. However, the device data only confirmed the first statement (e.g. 0.02 cd A^{-1} at luminance of 6 cd m^{-2} for **CuN1** versus 0.35 cd A^{-1} at luminance of 117 cd m^{-2} for **CuN2**), while **CuS2**-LECs surprisingly featured a very poor performance (0.04 cd A^{-1} at luminance of 10 cd m^{-2}) compared to, for example, those with **CuN2**. Thus, despite the well-known empirical design rules between the X-ray structural parameters and the photoluminescence behavior in powder are successful, they do not fully apply to understand the electroluminescent behavior in thin-film lighting.[27]

Herein, we rationalize this counterintuitive mismatch, capitalizing on a new multivariate analysis model that correlates the X-ray structural and electronic parameters of Cu-iTMCs with their photo-/electro-luminescent behaviors in thin-films applied to lighting.[27] Indeed, this model predicted **CuN2** / **CuS2** thin-film emission centered at 527 nm / 569 nm associated to ϕ of 8% / 23% and their respective devices with 0.25 cd A^{-1} at luminance of 94 cd m^{-2} / 0.08 cd A^{-1} at luminance of 12 cd m^{-2}, while the experimental values are 540 nm / 580 nm, 10% / 21%, and 0.35 cd A^{-1} at luminance of 117 cd m^{-2} / 0.04 cd A^{-1} at luminance of 10 cd m^{-2}, respectively. This behavior is primary ruled by the increased total polar surface area (tPSA) and partition coefficient (*c*log*P*) features. These parameters, traditionally used for the definition of the polarity and the lipophilicity[30,31] of organic molecules, are here used to describe the electronic changes using π-extended and S-bridged ligands, respectively. Electrochemical impedance spectroscopy (EIS) allowed us to rationalize the relevance of these parameters in terms of dielectric constant (ϵ) and ion conductivity (σ) features that rule the effective formation of EDLs and the growth of p-/n-doped regions. In short, **CuN2**-LECs featured the highest ϵ and σ compared to **CuS2/CuN1**-LECs (20.5 vs 14.6 / 5.12 and *s* of 58 vs 16 / 20 nS m^{-1}), suggesting that nonconventional rules for a good polarization ability are also paramount in designing N/S-bridged N^N ligands for Cu-iTMCs to ensure efficient in operando in ion-based lighting devices.

2. Results and Discussion

2.1. Synthesis and Characterization Protocols

CuN2 and **CuS2** were prepared following the previously procedure reported for the reference **CuN1** and **CuS1** with isolated yields of 92 and 67%, respectively – **Scheme 1**.[9] These complexes were fully characterized by ^{1}H, ^{13}C, ^{31}P, and ^{19}F NMR and high-resolution mass (HRMS) spectroscopies – Figures S1–S12 in the Supporting Information. Suitable single crystals were obtained by slow gas diffusion technique, using pentane as light solvent with a 1:1 diethyl ether:dichloromethane solution of **CuN2** and dichloromethane solution of **CuS2**. The X-ray analysis reveals that the π-extension of N^N ligand in **CuN2** and **CuS2** does not cause dramatic distortions in the complex structure compared to their respective references – **Figure 2** and **Table 1** and Table S1 (Supporting Information). All the P^P and N^N bite angles and Cu–P and Cu–N bonds distances are in the typical range of DPEPhos and dipyridyl ligands.[9,21,32–36] However, **CuN2** shows higher degree of asymmetry with respect of both, the references complexes and **CuS2** (i.e., $\Delta_{Cu-N1-Cu-N3}$ 0.06 Å / 0.04 Å / 0.02 Å / 0.02 Å for **CuN2** / **CuN1** / **CuS1** / **CuS2**), while the Cu···O distance is longer than 3.1 Å for all the complexes with the exception of **CuS1**, explaining its low ϕ in powder (<1%).[29]

E. Fresta
Institute for Molecular Engineering and Advanced Materials
INF 225
Universität Heidelberg
69120 Heidelberg, Germany

A. Montrieul, M. Linares
Division of Theoretical Chemistry
Department of Physics
Chemistry and Biology
Linköping University
Linköping SE-581 83, Sweden

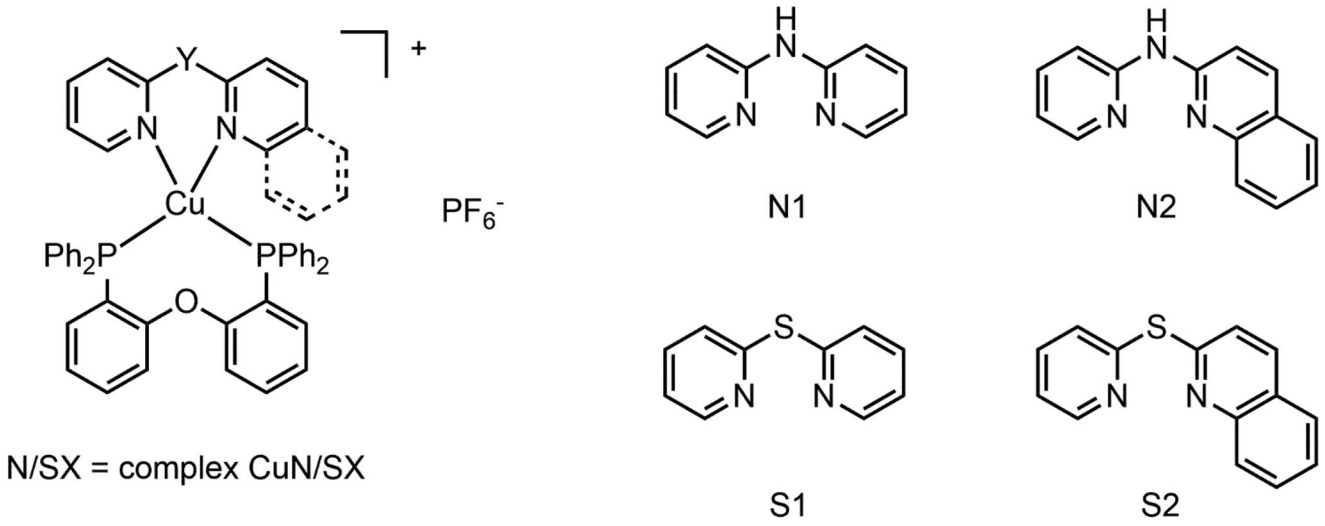

Figure 1. Chemical structures of complexes and ligands of this work.

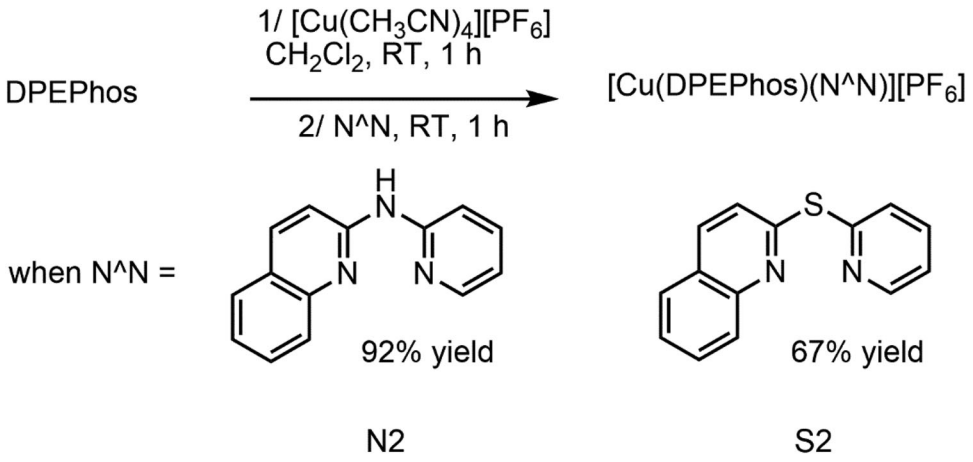

Scheme 1. Synthesis of **CuN2** and **CuS2** complexes.

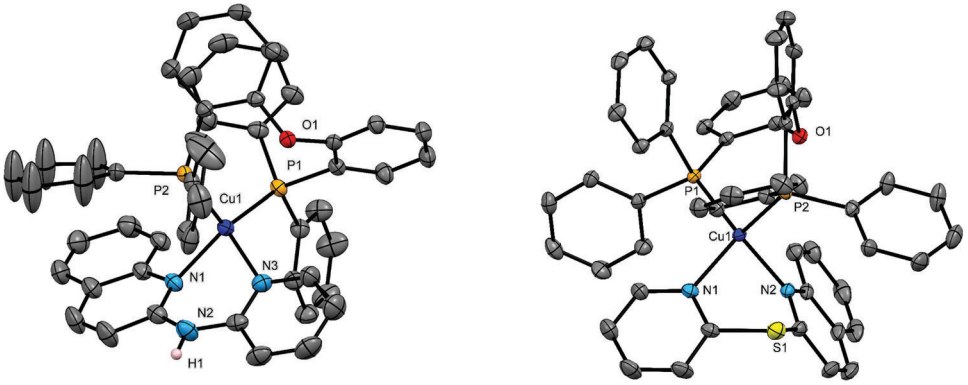

Figure 2. Ellipsoid representation (drawn at 50% probability level) of **CuN2** (left) and **CuS2** (right) from X-ray diffraction analysis. Hydrogen atoms and anions are omitted for clarity.

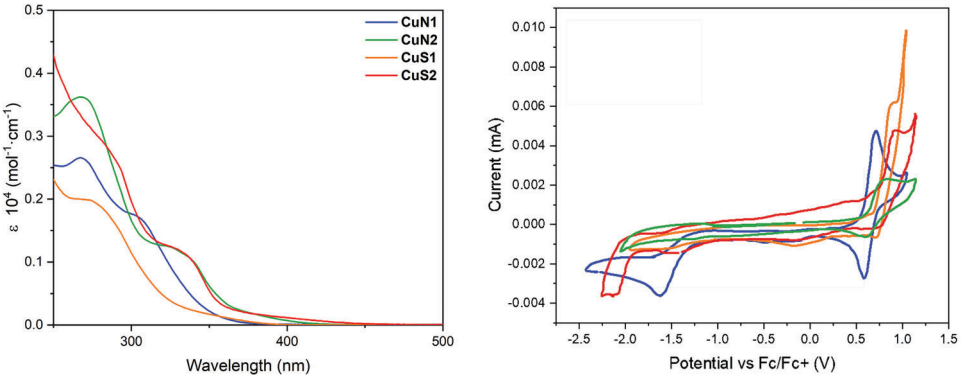

Figure 3. Left: UV–vis absorption spectra (2.5×10^{-3} M in CH_2Cl_2). Right: Cyclic voltammetry in CH_2Cl_2 (0.1 M of n-Bu_4NPF_6; scan rate 0.1 V s^{-1}) of the Cu-iTMCs.

2.2. Photophysical, Electrochemical, and Theoretical Studies

UV–vis spectroscopy was performed in dichloromethane solution – **Figure 3**, showing intense and broad absorption bands between 250 and 300 nm that are attributed to ligand-centered (LC) transitions, while metal-to-ligand charge transfer (MLCT) transitions are not observable as they are typically too weak.[9,17,21] More in detail, two main contributions can be identified: (i) LC absorption bands related to the $\pi \rightarrow \pi^*$ transitions of the DPEPhos ligand in the range of 250–275 nm [9,15,37,38] and (ii) LC transition related to the $\pi \rightarrow \pi^*$ transitions of the N^N ligands in the lower-energy region. Here, the presence of the π-extended electro-deficient heteroaromatic ring (**CuN2** / **CuS2** vs **CuN1** / **CuS1**) leads to a further red-shifted absorption features. This is in line with theoretical and electrochemical studies. On one hand, DFT/TD-DFT studies indicated a strong stabilization of the lowest unoccupied molecular orbital (LUMO) located at the N^N ligands and small stabilization of the highest occupied molecular orbital (HOMO) located at the Cu-P^P moiety using the π-extended ligands regardless of the bridged atom — Figures S13–S19 (Supporting Information) and **Table 2**. However, the use of S-bridged ligands strongly stabilized both frontier molecular orbitals compared to **CuN1/2** family. This leads to a synergistic reduction of the optical bandgap upon π-extended ligands and using a withdrawing S-bridged atom — Table 2. On the other hand, the electrochemical behavior was investigated by cyclic voltammetry of dichloromethane solutions versus Fc / Fc^+ – Table 2 and Figure 3. All the species feature an oxidation wave in the range between 0.64 and 0.95 V attributed to the Cu^+ / Cu^{2+} process,[39] showing three trends: (i) the oxidation potential is slightly increased using the π-extended ligands as the HOMO is stabilized, (ii) **CuN1/2** feature a lower oxidation potential compared to their respective **CuS1/2** due to the withdrawing effect of the sulfur atom,[17] and (iii) **CuN1/2** feature reversible oxidation waves, while the S-bridged ligand leads to irreversible (**CuS1**) and/or quasi-reversible (**CuS2**) oxidation processes.[9] Concerning the reduction process that is located at the N^N moiety as indicated by the theoretical description — vide supra, the π-extension of the ligand leads to significantly lower reduction potentials going, from example, from −1.59 to −1.35 V for **CuS1** and **CuS2** and enhances the reversibility of the reduction process for both family of complexes — Table 2.

While Cu(I)-iTMCs exhibit a very weak emission and low stability in solution,[16,17,40,41] they feature a strong emission in solid-state – i.e., powder and thin-film; **Figure 4** and

Table 1. Selected bonds (Å) and angles (°) of the complexes.

Complex	Cu–P [Å]	Cu–N [Å]	N^Cu^N [°]	P^Cu^P [°]	N^Cu^P [°]	Ref.
CuN1	2.2690(7) 2.2867(7)	2.050(2) 2.089(2)	91.59(8)	110.66(2)	106.77(7) 112.78(6) 113.96(6) 119.19(6)	[9]
CuN2	2.2485(8) 2.2714(8)	2.059(3) 2.117(2)	89.26(10)	113.23(3)	108.62(7) 110.61(8) 111.28(8) 121.33(7)	This work
CuS1	2.2582(8) 2.2877(8)	2.074(2) 2.094(2)	90.73(9)	112.93(3)	100.29(7) 112.67(8) 115.71(7) 121.75(7)	[9]
CuS2	2.2783(5) 2.2871(5)	2.1054(16) 2.1243(15)	91.20(6)	107.44(1)	106.58(4) 108.91(5) 116.41(4) 126.23(4)	This work

Table 2. Cyclic voltammetry for Cu(I)-iTMCs in dichloromethane.

Complex	E_{ox} [V]	E_{red} [V]	HOMO [eV]	LUMO [eV]	Ref.
CuN1	0.64, r[a)]	−1.63, qr[b)]	−5.44	−3.17	[9]
CuN2	0.75, r	−1.25, qr	−5.55	−3.55	This work
CuS1	0.81, irr[c)]	−1.59, irr	−5.61	−3.21	[9]
CuS2	0.95, qr	−1,35, qr	−5.75	−3.45	This work

[a)] r: reversible; [b)] qr: quasi-reversible; [c)] irr: irreversible.

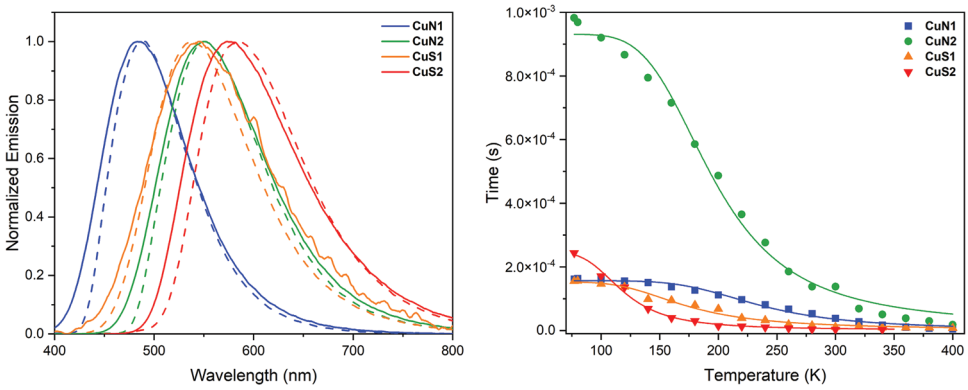

Figure 4. Left: Emission spectra at 298 K (solid lines) and 77 K (dashed lines) of powder samples. Right: τ in the range of 77–400 K fitted with Equation 1 (powder sample).

Figures S20–S27 (Supporting Information), and **Table 3**.[42] In powder, the complexes feature a broad emission band centered between 480 and 575 nm, spanning from the blue to yellow-orange region of the visible spectrum. In line with the description above,[9] ligands with the electron-withdrawing sulfur atom bathochromically shift the emission from 480 nm (**CuN1**) to 546 nm (**CuS1**). This is also synergistic upon using π-extended heteroaromatic **N2** and **S2** ligands, leading to complexes with a further red-shifted emission centered at 551 nm (**CuN2**) and 574 nm (**CuS2**). This is associated to ϕ values of ≈15% for the **CuN1/2** family, while it increases from <1% to 38% for **CuS1** and **CuS2**, since the **CuS1** features a shorter Cu···O distance – Tables 1 and 3.[29] In addition, the τ values are in the microsecond regime as expected for TADF emitters — Table 3. Owing to their small singlet–triplet energy splitting ($\Delta E_{S1/T1} < 0.12$ eV) and fast intersystem crossing (ISC) in Cu-iTMCs,[11–15] repopulation of the higher-lying S_1 state is allowed from the low-lying T_1 state at room temperature allowing to harvest all the electro-generated excitons. In this context, S_1 and T_1 geometries were optimized and the vertical transitions S_1–S_0 and T_1–S_0 were calculated together with the corresponding $\Delta E_{S1/T1}$ — Figure S19 in the Supporting Information. In this series, the $\Delta E_{S1/T1}$ value spans from 0.03 to 0.18 eV, indicating that a TADF emission mechanism could be involved. Thus, temperature-dependent steady-state and time-resolved spectroscopic experiments were carried out. Upon cooling down until 77 K, the two typical fingerprints of TADF mechanism were noted: (i) the E_{0-0} band of the emission peak red-shifts due to the deactivation of the reverse ISC (rISC) at low temperature and, in turn, prevalence of the $T_1 \rightarrow S_0$ decay mechanism is noted – **Table 4**, Figure 4 and Figures S20–S23 (Supporting Information),[35] and (ii) the τ drastically increase, being the high-lying S_1 not accessible anymore. As T_1 and S_1 states are mutually thermally equilibrated, the dependency of τ versus temperature follows a Boltzmann-type distribution described by Equation 1[19,35,37,43–45]

$$\tau_{em}(T) = \frac{3 + \exp\left(-\frac{\Delta E(S_1-T_1)}{k_B T}\right)}{\frac{3}{\tau(T_1)} + \frac{1}{\tau(S_1)}\exp\left(-\frac{\Delta E(S_1-T_1)}{k_B T}\right)} \quad (1)$$

where k_B is the Boltzmann constant, $\Delta E_{S1/T1}$ the energy separation between the two states, and $\tau(S_1)$ / $\tau(T_1)$ the excited state decay lifetime of prompt fluorescence/phosphorescence, respectively. A good fit ($R^2 > 0.99$) was achieved in all the cases and the fitted $\Delta E_{S1/T1}$ are in good agreement with the calculated ones. However, it is worth to note that all the complexes show a biexponential decay curve in the range between 77 and 298 K and the τ decays recorded at 298 K are too long to be attributed to a pure delayed fluorescence decay mechanism. Thus, it is possible to hypothesize coexistence of the TADF emission mechanism and residual phosphorescence at room temperature. To confirm this hypothesis we applied Equation 2, under the assumption that the absorption features are temperature-independent[38]

$$\frac{I(S_1)}{I(T_1)} = \frac{\tau(T_1)}{3\tau(S_1)}\exp\left(-\frac{\Delta E\,(S_1 - T_1)}{k_B T}\right) \quad (2)$$

Table 3. Photophysical data of Cu(I)-iTMCs in crystalline powder and thin-film.

	Powder								Thin Film					
Complex	λ_{em} 298 K [nm]	λ_{em} 77 K [nm]	τ_{av} 298 K [µs]	τ_{av} 77 K [µs]	ϕ [%]	k_r[a] [x 10^4 s^{-1}]	k_{nr}[a] [x 10^4 s^{-1}]	λ_{em} 298 K [nm]	λ_{em} 77 K [nm]	τ_{av} 298 K [µs]	τ_{av} 77 K [µs]	ϕ [%]	k_r[a] [10^4 s^{-1}]	k_{nr}[a] [10^4 s^{-1}]
CuN1	480	490	24.7	198.4	17	0.7	3.4	497	493	15.2	177.0	8	0.5	6.0
CuN2	551	549	7.31	982.4	14	1.9	11.8	540	537	61.9	781.0	10	0.2	1.5
CuS1	546	537	11.2	155.6	< 1	0.1	8.8	546	537	7.5	160.3	< 1	0.1	1.3
CuS2	574	584	3.0	244.1	38	12.7	20.7	580	571	47.6	944.0	21	0.4	1.7[a]

[a] calculated from τ and ϕ values measured at 298 K.

Table 4. Experimental and theoretical parameters of TADF emission mechanism for Cu(I)-iTMCs in powder and thin-film.

Complex	ΔE (S_1/T_1) calc. [eV]	ΔE (S_1/T_1) sper. [eV]	77 K		300 K			
			Power and thin-film		Powder		Thin-film	
			I (T_1)	I (S_1)	I (T_1)	I (S_1)	I (T_1)	I (S_1)
CuN1	0.1026	0.1179	>99%	< 1%	15%	85%	15%	85%
CuN2	0.1804	0.0958	>99%	< 1%	13%	87%	11%	89%
CuS1	0.0530	0.0729	>99%	< 1%	23%	77%	8%	92%
CuS2	0.0353	0.0620	96%	4%	3%	97%	7%	93%

where $I(S_1)$ is the TADF intensity originated from the singlet state S_1 and $I(T_1)$ the phosphorescence intensity from the triplet state T_1. Consequently, the contribution of TADF mechanism at room temperature spans from ≈85% (**CuN1**/**2**) and 77% (**CuS1**), while **CuS2** show a higher efficiency of the TADF process – Table 4. In overall, the combination of π-extended ligands and S-bridged atoms leads to an enhanced radiative rate constant, ϕ, and TADF yield, suggesting **CuS2** as the best emitter for LECs, while only the π-extension does not provide a significant photoluminescence improvement, pointing out that **CuN1** and **CuN2**-devices should perform alike.

To further confirm this statement, we must consider that LECs are thin-film based technology and Cu(I)-TMCs are prone to unforeseen geometrical changes upon solution-based fabrication techniques leading to significant modifications of the photoluminescent features in thin-films — Figures S24–S27 (Supporting Information); Tables 3 and 4.[27] Thus, we decided to carry out similar studies in thin-films applied to LECs. Thin-films (80–100 nm) were prepared on quartz slides via spin-coating of a 20 mg mL^{-1} butan-2-one solution. Atomic force microscopy (AFM) images of previously reported **CuN1** and **CuS1**,[9] as well as those of their respective π-extended system-complexes, showed a similar homogeneous morphology with root mean square roughness (RMS) values < 1 nm – Figure S28 (Supporting Information) – that is suitable for both photophysical studies and device fabrication. In thin-films, the structural design of the ligands led to the same trends with respect to emission shifts and ϕ – Table 3. Similar to what has been described in crystalline powder, all the complexes retain an analogous TADF emission mechanism in thin-films — Figures S24–S27 (Supporting Information) and Table 4. Indeed, $\Delta E_{S1/T1}$ values are in line with the theoretical values and the TADF versus phosphorescence rate contributions at the room temperature slightly changes compared to those in crystalline powder. This suggests that the above discussed conclusions hold in thin-films with respect to the device performance expectations based on the photoluminescent behavior of this series of complexes.

2.3. Electroluminescent Studies

LECs were fabricated with a double-layered architecture ITO/PEDOT:PSS (70 nm)/active layer (80–100 nm)/Al (90 nm), in which PEDOT:PSS is poly(3,4-ethylenedioxythiophene) polystyrene sulfonate, the active area was 10 mm^2, and the driving conditions were 1 kHz block wave and 50% duty cycle at 5 mA pulsed current compliance.[6,28] As already reported, **CuN1**-devices showed a broad greenish emission band centered at 523 nm – Figure S29 (Supporting Information) and **Table 5**, while **CuS1**-LECs showed no luminescence.[9] In contrast, both **CuN2**- and **CuS2**-devices featured an intense green or orange electroluminescence centered at 562 and 577 nm that corresponds to x/y CIE color coordinates of 0.38/0.53 and 0.49/0.49, respectively — Figure S30 in the Supporting Information. Here, the photo-/electro-luminescence band shapes are the same –, i.e., E_{0-0} of 2.88 eV / 2.63 eV and full width at half maximum of 110 nm / 90 nm for **CuN2** / **CuS2**, respectively, indicating that the same excited state is involved regardless of the photo/electrical excitation stimuli. In addition, the spectra shape is fairly stable for the entire device lifespan — Figure S30 in the Supporting Information.

Worth to note is the typical LEC behavior of **CuN2**-devices with an instantaneous luminance value of ≈10 cd m^{-2} that increases up to 117 cd m^{-2} (0.35 cd A^{-1}) and an initial average voltage (≈8 V) that exponentially reduces to a plateau of 5.5 V – **Figure 5**. The quick decrease of the average voltage is related to the electrochemical doping promoted by the formation of EDLs at the electrode interface, while the voltage plateau indicates the lack of a severe electrochemical degradation (over oxidation/reduction processes). In contrast, **CuN1**-devices featured a similar LEC behavior, reaching a very poor device performance of 0.02 cd A^{-1} at luminance of 6 cd m^{-2} that is in line with the previous reports.[9] Overall, **CuN2**-devices are surprisingly outperforming **CuN1**-devices when both complexes featured a similar photoluminescence behavior — vide supra. What is more striking, **CuS2**-LECs displayed a similar poor device performance to that noted for **CuN1**-LECs. In short, a small initial rise of the average voltage profile followed by a subsequent exponential drop is attributed to a slow kinetics of EDLs formation. Thus, the nonoptimal EDLs formation leads to a poor luminance level, reaching 0.04 cd A^{-1} at luminance of 10 cd m^{-2}. Since the voltage profiles slightly differ each other, a direct comparison of the reached luminance is not exhaustive, therefore, power conversion efficiencies (PCE) and external quantum efficiency (EQE) have been calculated and discussed. In detail, while **CuN1**- and **CuS2**-based LECs exhibited PCE of 0.03 lm W^{-1}, **CuN2**-LECs recorded an order of magnitude improvement (i.e., 0.11 lm W^{-1}). Similarly, the EQE values are 0.13% / 0.02% / 0.01% for **CuN2**- / **CuS2**- / **CuN1**-LECs, respectively — Figure S31 in the Supporting Information. The EQE of LECs can be estimated following Equation 3[46,47]

$$\mathrm{EQE} = \gamma \times \eta_{s,t} \times \phi \times \eta_{out} \times \left(1 - X_{loss}\right) \quad (3)$$

Table 5. Figure-of-merits of **CuN1**, **CuN2**, **CuS1** and **CuS2** devices and EIS parameters.

Complex	L_{max} [cd m^{-2}]	$t_{½}$ [min]	Eff [cd A^{-1}]	PCE [lm W^{-1}]	C_{eff} [nF]	ϵ	σ [S m^{-1}]	λ_{em} [nm]	x/y CIE color coordinates
CuN1	6	1.1	0.02	0.03	6.13	5.12	2.02×10^{-8}	523	0.26/0.38
CuN2	117	1.8	0.35	0.11	12.1	20.5	5.77×10^{-8}	562	0.38/0.53
CuS1	–	–	–	–	4.4	4.5	3.0×10^{-9}	–	–
CuS2	10	2.4	0.04	0.03	7.16	14.6	1.60×10^{-8}	577	0.49/0.49

Where γ is the recombination efficiency (equal to 1 for LECs devices in which two Ohmic contact are established), $\eta_{s,t}$ is the spin factor (equal to 1 for TADF emitters),[46] η_{out} is the out-coupling efficiency (for flat substrate can be approximate with $1/(2n^2)$, with n the refractive index of the glass substrate), and X_{loss} is the loss factor that take into account additional efficiency losses, such as exciton quenching due to temperature reached in operando, close proximity of emissive zone to doped front and/or polarons, among others.[46]

Taking into account the ϕ values (**CuN1** ≈ **CuN2**; **CuS2** > **CuN2**/**CuN1** – Table 3) is possible to estimate that the loss pathways for **CuS2**- / **CuN1**-based LECs are dramatically higher than that of **CuN2**-devices.

The explanation of such counterintuitive LEC behavior is not trivial, since no direct correlation between the structural, electrochemical, and photophysical parameters with the electroluminescent behavior is apparent. To shed light on this unexpected finding, we capitalized on the information derived from a multivariate analysis correlating X-ray structural and electronic parameters in a large dataset (>90 contributions) of luminescent Cu(I)-iTMCs applied in LECs and OLEDs focusing on two outputs, namely ϕ in thin-film and device efficiency.[27] At first, the implementation of the structural and electronic parameters of the new complexes to the model led to a good statistical correlation ($R^2 > 92$), leading to experimental and predicted match. In short, the predicted **CuN1**/ **CuN2** / **CuS2** thin-film emission is centered at 511 nm / 527 nm / 569 nm associated to ϕ of 6% / 8% / 23% and their respective devices with 0.01 cd A^{-1} at luminance of 6 cd m^{-2} / 0.25 cd A^{-1} at luminance of 94 cd m^{-2} / 0.08 cd A^{-1} at luminance of 12 cd m^{-2}, while the experimental values are 497 nm / 540 nm / 580 nm, 8% / 10% / 21%, and 0.02 cd A^{-1} at luminance of 6 cd m^{-2} / 0.35 cd A^{-1} at luminance of 117 cd m^{-2} / 0.04 cd A^{-1} at luminance of 10 cd m^{-2}, respectively. Next, the mismatch between photo- and electro-luminescent data can be understood by questioning the model about the first and second order interactions that rule, for example, the ϕ and device efficiency in this series. Here, the former is strongly influenced by the Cu···O distance, buried volume (% V_{bur}), and *clogP* of the N^N ligand as top three first order interactions — Figure S32 (Supporting Information), while the latter is ruled by LUMO, tPSA, and Cu···O distance as first order interactions. Thus, no straight correlation should be expected.

To highlight the relevance of tPSA and clogP parameters on ϕ and device efficiency, **Figure 6** confirms their large impact (i.e., 1 order of magnitude window between max. and min. values) on both outputs, keeping a good match between predicted and experimental data for each complex. What is more, the model suggests that high clogP seems to be beneficial for both, ϕ and device efficiency. In contrast, the device efficiency is mainly enhanced with ligands featuring a low tPSA value. This nicely translates to the chemical design, since the S-bridge strategy leads to an almost twofold increase in the tPSA value –, i.e. 37 (**CuN2**) versus 51 (**CuS2**), while the *clogP* goes from 3.21 **CuN2**, to 2.99 **CuS2**, and to 1.89 **CuN1**; a trend in perfect correlation with ϕ in thin-films (Table 3) and the device performance (Table 5). Finally, the physical meaning of these parameters with respect to the device mechanism must be understood. Since they are related to electronic and polarization effects on the complexes, we decided to study the device working mechanism with respect to ϵ and σ features via static EIS technique. In detail, we imposed a DC voltage spanning from 0 to 5 V to an AC signal of 10 mV amplitude and at frequencies from 10^6 to 10^0 Hz.[48–52] The Nyquist plots were analyzed using a single resistor/capacitor equivalent circuit – Figures S33–S35 in the Supporting Information.[53,54]

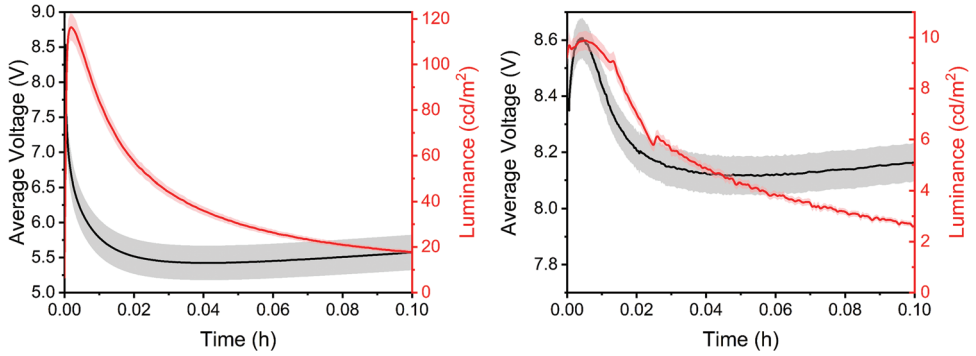

Figure 5. Average voltage (black) and luminance (red) versus time for **CuN2** (left) and **CuS2** (right) based devices measured at pulsed applied current of 5 mA.

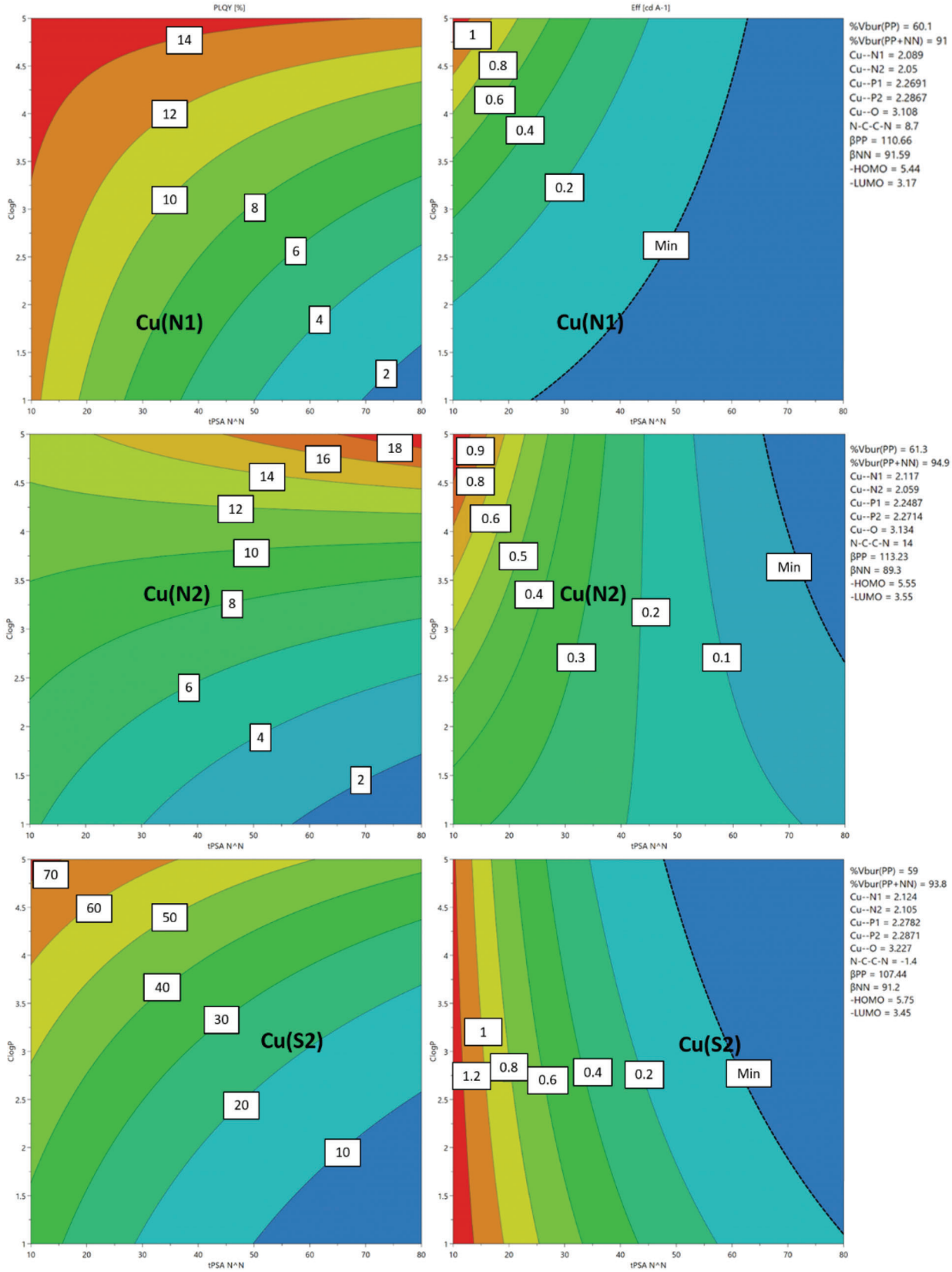

Figure 6. Contour plots of ϕ (left) and device efficiency (right) of **CuN1** (top), **CuN2** (middle), and **CuS2** (bottom), highlighting the effect of *c*log*P* (*y*-axis) and tPSA (*x*-axis) in the corresponding experimental space. The relative position of each complex is depicted by the corresponding label.

In particular, ϵ and σ are univocally determinated at applied DC voltage 0 V.[55] As gathered in Table 5, ϵ of **CuN1/S1** (5.12/4.6) is much smaller than **CuN2** (20.5) and **CuS2** (14.6), indicating that π-extended heteroaromatic system is beneficial for the formation of the EDLs, while the implementation of S-bridge is detrimental for the ion conductivity affecting the growing of the doped fronts – e.g. 5.77×10^{-8} (**CuN2**) versus 1.60×10^{-8} S m^{-1} (**CuS2**). Thus, the best balance between ϵ and σ is provided in devices with **CuN2** that are best performing in this series, despite its photoluminescent features — vide supra. Thus, the above electronic/polarization features of the ligands must also be taken into account when designing coordination complexes for ion-based optoelectronics.

3. Conclusion

Herein, we rationalize a counterintuitive mismatch between the common chemical design to provide highly emissive low-energy Cu-iTMCs (i.e., π-extension and heteroatom-bridge) and the lack of success to result in efficient low-energy LECs. This is related to a nonobvious design thought about the need to take into account the ligand polarization features (i.e., *c*log*P* and tPSA) that rule ϵ and σ in thin-films and, in turn, the device operation mechanism. This was revealed by a multivariate analysis model correlating X-ray structural and electronic parameters of Cu-iTMCs with their photo-/electro-luminescent behaviors in thin-films applied to lighting and EIS study. In short, the π-extension enhances both the photoluminescent figures-of-merit as well as the ϵ and σ parameters that are key towards high performing LECs. In contrast, the combination of π-extension and S-bridge approaches synergistically leads to complexes with, for example, the highest ϕ, but the ϵ and σ parameters are significantly reduced, compromising the device performance. Thus, polarizability of the ligands must be considered along with the well-known structural parameters to design Cu(I)-iTMCs toward highly performing ion-based lighting devices.

4. Experimental Section

Synthesis: All the commercially available compounds were purchased and used without further purification. All the reactions were performed under dry argon atmosphere, using standard Schenk technique. Purchased solvents were degassed bubbling Ar directly in bulk. ^{1}H, ^{13}C, ^{31}P, and ^{19}F NMR spectra were recorded at 298 K on 500 and 600 MHz Brüker spectrometers and they are reported in the following format: multiplicity (s, singlet; d, doublet; t, triplet; q, quartet; qui, quintet; sex, sextet; sept, septet; m, multiplet), coupling constant(s) (*J*) in Hertz (Hz), number of protons. The prefix "br" is occasionally used in case of broad signals. HRMS were performed by LCMT analytical service (See the Supporting Information).

Crystallography: Crystallographic data sets were collected from single-crystal samples, performing the analysis with a Brüker Kappa APEXII CCD diffractometer. The initial unit cell parameters were determined by a least-squares fit of the angular setting of strong reflections, collected by a 6.0° scan in 12 frames over three different parts of the reciprocal space (36 frames total). Cell refinement and data reduction were performed with SAINT (Brüker AXS). Absorption correction was done by a multiscan method using SADABS 2012/1 (Brüker AXS). The structure was solved by direct method and refined using SHELXL-97 or SHELXL-2013 (Sheldrick). All non-H atoms were refined by full-matrix least-squares with anisotropic displacement parameters while hydrogen atoms were placed in idealized positions. The short interactions were calculated using the software Platon version 250 420.

Photophysical Measurements: UV–vis absorption spectra were collected at room temperature from 2.5×10^{-3} M solution in CH_2Cl_2 on a PerkinElmer Lambda 40 UV-visible spectrometer. Wavelengths are reported in nanometers (nm) and the molar extinction coefficients (ϵ) in L mol^{-1} cm^{-1}. Steady-state emission spectra and emission quantum yield (ϕ) were measured with FS5 Spectrofluorometer (Edinburgh Instruments). The measurements of the time-resolved photoluminescence were performed using Multi-Channel Scaling (MCS) as photocounting method and pulsed µs Xe-flash lamp as excitation source (Edinburgh Instruments, FS5 Spectrofluorometer). For temperature-dependent measurements, the FS5 Spectrofluorometer (SC-80 holder) was equipped with an optical cryostat (Optistat-DN, Oxford Instruments). The intensity-weighted intensity lifetime was used in the case of biexponential decays of the excited state.[56]

Electrochemistry: Cyclic voltammetry experiments were carried out at room temperature under inert atmosphere with Autolab PGSTAT101 an electrochemical analyzer potentiostat unit from Metrohm with the Nova software package version 2.1. The cell (standard three-electrode configuration) was set up using a glassy-carbon electrode as working electrode, platinum wire and Ag/AgCl as, respectively, auxiliary and reference electrode. The measurements were recorded at a scan rate of 0.1 V s^{-1} and step potential of 0.00244 V. Cu(I) complexes were analyzed in anhydrous and degassed solution of CH_2Cl_2 (0.1 M) of n-Bu_4NPF_6. The electrodes were calibrated using a solution of ferrocene ($Fc/Fc^+ = 0.46$ V).

Device Preparation and Characterization: Indium–tin oxide (ITO) substrates were purchased from Naranjo Substrates with an ITO thickness of 130 nm. The cleaning of the substrates is composed to four steps: water diluted Derquim detergent (ratio 1:1 v/v), distilled water, ethanol and propan-2-ol as solvents in a warm ultrasonic bath (60 °C, 37–70 Hz) for 15 min each step. Then, the substrates were dried in N_2 flow and treated in a UV-ozone cleaner for 8 min. The aqueous PEDOT:PSS solution (Clevios P VP.AI4083) was diluted with propan-2-ol (ratio 3:1 v/v). The resulting solution was sonicated at room temperature for 15 min and then filtered through a (0.45 µm pores diameter) before the spin-coating onto the clean substrates. The resulting layers were dried on a heating plate at 120 °C and stored in the glovebox (N_2 atmosphere, <0.1 ppm O_2 and H_2O, Angstrom Engineering). The complexes were dissolved in butan-2-one, reaching the concentration of 20 mg mL^{-1}. The solutions were sonicated for 10 min and filtered before the deposition. The films were prepared by spin-coating of 60 µL of solution at 2000 rpm for 60 s, reaching thick layers between 80 and 100 nm. Then, the active layers were dried in vacuum overnight. The AFM of the resulting samples was performed with MFP-3D Origin+ Oxford Instruments to confirm the suitable morphology of the layers. Finally, the aluminum cathode was deposited onto the active layer via physical vapor deposition (Ångstrom Covap evaporator integrated with the glovebox, $<1 \times 10^{-6}$ mbar). A shadow mask was used to define 4 pixels with an area 10 mm^2 per substrate. Voltage and current performances of the devices were evaluated with Botest OLT OLED Lifetime-Test System operating in pulsed mode. The ITO is used as anode while the aluminum as cathode. LECs were connected to the measuring unit via gold coated spring loaded pins. Time dependence of luminance and the electroluminescence spectra were recorded with Avantes spectrophotometer (AvaspecULS2048L-USB2) equipped with a calibrated integrated sphere Avasphere 30-Irrad. Metrohm µAutolabIII potentiostat/galvanostat equipped with a frequency analyzer module (FRA2) was used to carry out EIS assays. The range of the applied was set between 0 and 5 V and fitted (Nova 2.1) with the equivalent circuit model reported in Figure S33 in the Supporting Information.

Multivariate Tools: The software MODDE 13 (Umetrics) was used. The authors defined 15 factors in total, namely: percent buried volume of P^P ligand (%V_{bur} PP) and percent buried volume of complex (%V_{bur} PP+NN), distances between Cu–N1, Cu–N2 (with Cu–N1 > Cu–N2), Cu–P1, Cu–P2 (with Cu–P1 < Cu–P2), Cu···O, torsion angle of the N^N ligand, total polar surface area of the ligand N^N (tPSA N^N), predicted partition coefficient (*c*log*P*), bite angles of P^P and N^N ligands, HOMO and LUMO levels, and type of optoelectronic device (OLED or LEC). The database was fitted with PLS method considering both first and second order terms. First-order

terms consider the single factors independently, while second-order ones refer to interaction between factors.

Statistical Analysis: Thin films statistics involve three replicates for each composition, whereas device statistics involve up to 20 devices. The *t*-test was used to confirm the absence of outliers. The values reported in the manuscript are the average ones and the histogram is presented in Figure S31 in the Supporting Information. For data processing and evaluation, the software OriginPro 2020b was employed.

[CCDC 2 257 839 and 2 257 840 contain the supplementary crystallographic data for this paper. These data can be obtained free of charge from The Cambridge Crystallographic Data Centre via www.ccdc.cam.ac.uk/data_request/cif].

Supporting Information

Supporting Information is available from the Wiley Online Library or from the author.

Acknowledgements

G.G. and L.M.C. contributed equally to this work. L.M.C. and R.R. acknowledge the European Union under grant agreement MSCA-ITN STiBNite No. 956923. This work was supported by the "Ministère de l'Enseignement Supérieur et de la Recherche", CNRS (Centre National de la Recherche Scientifique) and the LABEX SynOrg (ANR-11-LABX-0029). S.G. acknowledges the "Région Normandie" (G.G.), the Graduate School of Research XL-Chem (ANR-18-EURE-0020 XL-Chem) (A.M.) and Normandie University (G.U.M.) for their fundings.

Open access funding enabled and organized by Projekt DEAL.

Conflict of Interest

The authors declare no conflict of interest.

Data Availability Statement

The data that support the findings of this study are available from the corresponding author upon reasonable request.

Keywords

copper (I) complexes, light-emitting electrochemical cells, multivariate analysis, thermally activated delayed fluorescence, thin-film lighting

Received: April 27, 2023
Revised: July 18, 2023
Published online: August 22, 2023

[1] A. Sandström, A. Asadpoordarvish, J. Enevold, L. Edman, *Adv. Mater.* **2014**, *26*, 4975.
[2] R. D. Costa, E. Ortí, H. J. Bolink, F. Monti, G. Accorsi, N. Armaroli, *Angew. Chem., Int. Ed.* **2012**, *51*, 8178.
[3] Q. Pei, G. Yu, C. Zhang, Y. Yang, A. J. Heeger, *Science* **1995**, *269*, 1086.
[4] J. Ràfols-Ribé, E. Gracia-Espino, S. Jenatsch, P. Lundberg, A. Sandström, S. Tang, C. Larsen, L. Edman, *Adv. Opt. Mater.* **2021**, *9*, 2001405.
[5] S. Tang, A. Sandström, P. Lundberg, T. Lanz, C. Larsen, S. van Reenen, M. Kemerink, L. Edman, *Nat. Commun.* **2017**, *8*, 1190.
[6] E. Fresta, R. D. Costa, *J. Mater. Chem. C* **2017**, *5*, 5643.
[7] Q. Pei, Y. Yang, G. Yu, C. Zhang, A. J. Heeger, *J. Am. Chem. Soc.* **1996**, *118*, 3922.
[8] Q. Sun, Y. Li, Q. Pei, *J. Disp. Technol.* **2007**, *3*, 211.
[9] G. U. Mahoro, E. Fresta, M. Elie, D. di Nasso, Q. Zhang, J.-F. Lohier, J.-L. Renaud, M. Linares, R. Wannemacher, J. Cabanillas-Gonzalez, R. D. Costa, S. Gaillard, *Dalton Trans.* **2021**, *50*, 11049.
[10] E. Fresta, G. U. Mahoro, L. M. Cavinato, J.-F. Lohier, J.-L. Renaud, S. Gaillard, R. D. Costa, *Adv. Opt. Mater.* **2022**, *10*, 2101999.
[11] G. U. Mahoro, J. Fernandez-Cestau, J.-L. Renaud, P. B. Coto, R. D. Costa, S. Gaillard, *Adv. Opt. Mater.* **2020**, *8*, 2000260.
[12] C. E. Housecroft, E. C. Constable, *Coord. Chem. Rev.* **2017**, *350*, 155.
[13] N. Armaroli, H. J. Bolink, *Top. Curr. Chem.* **2016**, *374*, 44.
[14] C. E. Housecroft, E. C. Constable, *J. Mater. Chem. C* **2022**, *10*, 4456.
[15] R. Czerwieniec, M. J. Leitl, H. H. H. Homeier, H. Yersin, *Coord. Chem. Rev.* **2016**, *325*, 2.
[16] F. Wu, H. Tong, K. Wang, Z. Wang, Z. Li, X. Zhu, W.-Y. Wong, W.-K. Wong, *J. Photochem. Photobiol., A* **2016**, *318*, 97.
[17] C. M. Brown, C. Li, V. Carta, W. Li, Z. Xu, P. H. F. Stroppa, I. D. W. Samuel, E. Zysman-Colman, M. O. Wolf, *Inorg. Chem.* **2019**, *58*, 7156.
[18] B. Pashaei, S. Karimi, H. Shahroosvand, P. Abbasi, M. Pilkington, A. Bartolotta, E. Fresta, J. Fernandez-Cestau, R. D. Costa, F. Bonaccorso, *Chem. Soc. Rev.* **2019**, *48*, 5033.
[19] C. L. Linfoot, M. J. Leitl, P. Richardson, A. F. Rausch, O. Chepelin, F. J. White, H. Yersin, N. Robertson, *Inorg. Chem.* **2014**, *53*, 10854.
[20] S. Wang, C. Bruneau, J.-L. Renaud, S. Gaillard, C. Fischmeister, *Dalton Trans.* **2019**, *48*, 11599.
[21] E. Fresta, M. D. Weber, J. Fernandez-Cestau, R. D. Costa, *Adv. Opt. Mater.* **2019**, *7*, 1900830.
[22] M. D. Weber, M. Viciano-Chumillas, D. Armentano, J. Cano, *R. D. Costa Dalton Trans.* **2017**, *46*, 6312.
[23] S. Keller, F. Brunner, J. M. Junquera-Hernández, A. Pertegás, M.-G. La-Placa, A. Prescimone, E. C. Constable, H. J. Bolink, E. Ortí, C. E. Housecroft, *ChemPlusChem* **2018**, *83*, 217.
[24] S. Keller, A. Prescimone, H. Bolink, M. Sessolo, G. Longo, L. Martínez-Sarti, J. M. Junquera-Hernández, E. C. Constable, E. Ortí, C. E. Housecroft, *Dalton Trans.* **2018**, *47*, 14263.
[25] M. D. Weber, C. Garino, G. Volpi, E. Casamassa, M. Milanesio, C. Barolo, R. D. Costa, *Dalton Trans.* **2016**, *45*, 8984.
[26] F. Brunner, A. Babaei, A. Pertegás, J. M. Junquera-Hernández, A. Prescimone, E. C. Constable, H. J. Bolink, M. Sessolo, E. Ortí, C. E. Housecroft, *Dalton Trans.* **2019**, *48*, 446.
[27] L. M. Cavinato, S. Wölfl, A. Pöthig, E. Fresta, C. Garino, J. Fernandez-Cestau, C. Barolo, R. D. Costa, *Adv. Mater.* **2022**, *34*, 2109228.
[28] E. Fresta, R. D. Costa, *Adv. Funct. Mater.* **2020**, *30*, 1908176.
[29] S. Keller, M. Alkan-Zambada, A. Prescimone, E. C. Constable, C. E. Housecroft, *Crystals* **2020**, *10*, 255.
[30] A. Leo, C. Hansch, D. Elkins, *Chem. Rev.* **1971**, *71*, 525.
[31] S. Prasanna, R. J. Doerksen, *Curr. Med. Chem.* **2009**, *16*, 21.
[32] D. G. Cuttell, S.-M. Kuang, P. E. Fanwick, D. R. McMillin, R. A. Walton, *J. Am. Chem. Soc.* **2002**, *124*, 6.
[33] R. D. Costa, D. Tordera, E. Ortí, H. J. Bolink, J. Schönle, S. Graber, C. E. Housecroft, E. C. Constable, J. A. Zampese, *J. Mater. Chem.* **2011**, *21*, 16108.
[34] M. Alkan-Zambada, S. Keller, L. Martínez-Sarti, A. Prescimone, J. M. Junquera-Hernández, E. C. Constable, H. J. Bolink, M. Sessolo, E. Ortí, C. E. Housecroft, *J. Mater. Chem. C* **2018**, *6*, 8460.
[35] R. Czerwieniec, H. Yersin, *Inorg. Chem.* **2015**, *54*, 4322.
[36] G. M. Adams, A. S. Weller, *Coord. Chem. Rev.* **2018**, *355*, 150.
[37] R. Czerwieniec, J. Yu, H. Yersin, *Inorg. Chem.* **2011**, *50*, 8293.
[38] H. Yersin, A. F. Rausch, R. Czerwieniec, T. Hofbeck, T. Fischer, *Coord. Chem. Rev.* **2011**, *255*, 2622.

[39] A. Cinquantini, G. Opromolla, P. Zanello, *J. Chem. Soc., Dalton Trans.* **1991**, *11*, 3161.
[40] M. W. Mara, K. A. Fransted, L. X. Chen, *Coord. Chem. Rev.* **2015**, *2*, 282.
[41] O. Green, B. A. Gandhi, J. N. Burstyn, *Inorg. Chem.* **2009**, *48*, 5704.
[42] M. Iwamura, S. Takeuchi, T. Tahara, *J. Am. Chem. Soc.* **2007**, *129*, 5248.
[43] R. Czerwieniec, K. Kowalski, H. Yersin, *Dalton Trans.* **2013**, *42*, 9826.
[44] M. J. Leitl, V. A. Krylova, P. I. Djurovich, M. E. Thompson, H. Yersin, *J. Am. Chem. Soc.* **2014**, *136*, 16032.
[45] J. C. Deaton, S. C. Switalski, D. Y. Kondakov, R. H. Young, T. D. Pawlik, D. J. Giesen, S. B. Harkins, A. J. M. Miller, S. F. Mickenberg, J. C. Peters, *J. Am. Chem. Soc.* **2010**, *132*, 9499.
[46] S. Tang, P. Lundberg, Y. Tsuchiya, J. Ràfols-Ribé, Y. Liu, J. Wang, C. Adachi, L. Edman, *Adv. Funct. Mater.* **2022**, *32*, 2205967.
[47] S. Jenatsch, L. Wang, N. Leclaire, E. Hack, R. Steim, S. B. Anantharaman, J. Heier, B. Ruhstaller, L. Penninck, F. Nüesch, R. Hany, *Org. Electron.* **2017**, *48*, 77.
[48] A. Munar, A. Sandström, S. Tang, L. Edman, *Adv. Funct. Mater.* **2012**, *22*, 1511.
[49] A. Mishra, M. Alahbakhshi, R. Haroldson, L. D. Bastatas, Q. Gu, A. A. Zakhidov, J. D. Slinker, *Adv. Opt. Mater.* **2020**, *8*, 2000226.
[50] S. van Reenen, R. A. J. Janssen, M. Kemerink, *Adv. Funct. Mater.* **2012**, *22*, 4547.
[51] S. van Reenen, M. Kemerink, in *Light-Emitting Electrochemical Cells*, (Ed: R. D. Costa) Springer International Publishing, Cham **2017**, pp. 3–45.
[52] L. M. Cavinato, G. Millán, J. Fernández-Cestau, E. Fresta, E. Lalinde, J. R. Berenguer, R. D. Costa, *Adv. Funct. Mater.* **2022**, *32*, 2201975.
[53] S. B. Meier, D. Hartmann, A. Winnacker, W. Sarfert, *J. Appl. Phys.* **2014**, *116*, 104504.
[54] S. B. Meier, D. Hartmann, D. Tordera, H. J. Bolink, A. Winnacker, W. Sarfert, *Phys. Chem. Chem. Phys.* **2012**, *14*, 10886.
[55] B. M. D. Puscher, M. F. Aygüler, P. Docampo, R. D. Costa, *Adv. Energy Mater.* **2017**, *7*, 1602283.
[56] A. Sillen, Y. Engelborghs, *Photochem. Photobiol.* **1998**, *67*, 475.